ADVANCED FUNCTIONAL MATERIALS
www.afm-journal.de

Seed-Induced Vertical Growth of 2D Bi_2O_2Se Nanoplates by Chemical Vapor Transport

*Zhen Wu, Guoliang Liu, Yuxi Wang, Xin Yang, Tianqi Wei, Qianjin Wang, Jie Liang, Ning Xu, Zizhong Li, Bin Zhu, Heshan Qi, Yu Deng, and Jia Zhu**

As two-dimensional (2D) layered materials attract more attention owing to their unique optical, electrical, and thermal properties, there are persistent efforts to grow high-quality 2D layered materials for fundamental research and device applications. While large-area 2D layered materials with high crystal quality can be obtained through chemical vapor transport, the strong binding between 2D layered materials and substrates poses a significant challenge for attempts to reveal their intrinsic properties and to use these 2D building blocks for constructing advanced heterostructured devices. Therefore, it would be ideal to grow high-quality 2D materials with minimized contact and binding with substrate. Through both calculation and experiment, it is demonstrated that by introducing a seed layer at the nucleation stage, the crystallographic disregistry and the corresponding adhesion energy between 2D materials and substrate can be altered, resulting in a change of crystal surface in contact with the substrate, and therefore vertical growth of 2D materials on substrates. As an example, it is demonstrated that with Bi_2O_3 serving as a seed layer, vertical growth of 2D plates of Bi_2O_2Se on mica substrates can be realized. These vertically grown 2D nanoplates of Bi_2O_2Se can be conveniently transferred with their thermal properties investigated for the first time.

1. Introduction

Two-dimensional (2D) layered materials generate tremendous interest due to their unique properties at low dimension.[1–5] Chemical vapor transport has been one of the most important processes to grow various 2D layered materials with high crystal quality.[6–9] Because of the lowest binding energy between the exposed surface of 2D layered materials and substrate, the 2D layered materials typically tile on substrates during the growth.[10,11] While substrates sometimes can serve as mechanical support for 2D material-based devices, they often also pose as a significant challenge for both exploring the fundamental properties and developing 2D layered materials based applications. From a fundamental perspective, minimizing the effect from substrate is critical for revealing the intrinsic properties of 2D materials. For constructing advanced 2D based Van der Waals heterostructured devices, it is important but often quite challenging to conveniently transfer these 2D building blocks off the substrate without contamination[12–14] or degrading their crystal qualities.[15–17] Therefore, it is desirable to grow high-quality 2D layered materials with minimized binding with substrates. While there were a few earlier observations of vertical growth of 2D nanoplates on substrates, the growth mechanism remains elusive.[18–20] Understanding this mechanism can also lead to a generalized growth strategy of 2D nanoplates with minimized impact from substrates for the future development.

Bi_2O_2Se, which is emerging as one of the important 2D layered materials because of high mobility[21–28] and promising thermoelectric properties,[29–31] is taken as an example of demonstration here. In most of the previous studies, 2D nanoplates of Bi_2O_2Se were grown flatly on the freshly cleaved mica substrates (**Figure 1**a) by the chemical vapor deposition (CVD) method with high crystal quality, due to lattice matching between the Bi_2O_2Se and mica (Figure 1b). To explore their intrinsic thermal properties, it is often critical to transfer these 2D nanoplates to suspended substrates. However, it has been very challenging to transfer those Bi_2O_2Se 2D plates without degrading its crystal quality,[22,24,29] evidenced by their compromised mobility and mechanical properties once they were taken out of mica substrate.

Here in this work, we began with density functional theory (DFT) calculations to show that Bi_2O_3 can serve as seeds to change the growth orientation of Bi_2O_2Se nanoplates due to the variation of the crystallographic disregistry and the corresponding adhesion energy between the crystal surface of Bi_2O_2Se and Bi_2O_3. We then performed the experiment to demonstrate the successful vertical growth of high-quality Bi_2O_2Se nanoplates on mica substrates, assisted by Bi_2O_3 seed (Figure 1c,d). These vertical grown Bi_2O_2Se nanoplates can then be transferred mechanically to suspended substrates without

Dr. Z. Wu, Dr. G. Liu, Y. Wang, X. Yang, T. Wei, Q. Wang, J. Liang, N. Xu, Z. Li, Dr. B. Zhu, H. Qi, Dr. Y. Deng, Prof. J. Zhu
National Laboratory of Solid State Microstructures
College of Engineering and Applied Sciences
Jiangsu Key Laboratory of Artificial Functional Materials
Nanjing University
Nanjing 210093, P. R. China
E-mail: jiazhu@nju.edu.cn

The ORCID identification number(s) for the author(s) of this article can be found under https://doi.org/10.1002/adfm.201906639.

DOI: 10.1002/adfm.201906639

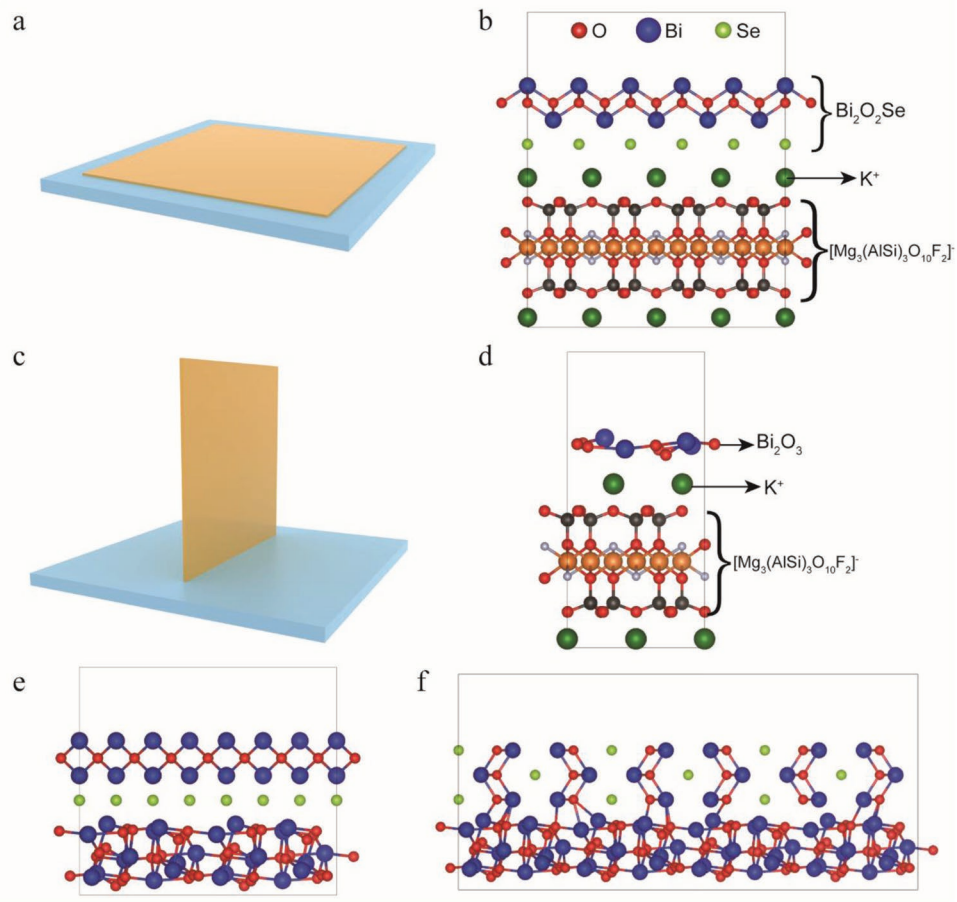

Figure 1. Schematic crystal structures of Bi_2O_2Se growing on substrate. a,c) Schematic diagrams of planar and vertical growth of Bi_2O_2Se on mica substrate. b) Surface crystal structure of planar growth of Bi_2O_2Se on mica stacked by mica-(001) surface and Bi_2O_2Se-(001) surface along the c-axis. d) Surface crystal structure of Bi_2O_3 growing on mica stacked by Bi_2O_3-(111) surface and mica-(001) surface along c-axis. e,f) Surface crystal structures staked by Bi_2O_2Se-(001) and Bi_2O_2Se-(100) surfaces with Bi_2O_3-(111) surface along c-axis, respectively.

contamination.[32] As a result, the intrinsic thermal properties of Bi_2O_2Se nanoplates can be revealed for the first time. It is found that thermal conductivity is about 1 W m^{-1} K^{-1} for the Bi_2O_2Se nanoplates narrow ribbon (300 nm wide, 26.8 nm thick, and 5.2 µm long), promising for thermoelectric applications.

2. Results and Discussion

As shown in Figure 1b, the planar growth of Bi_2O_2Se nanoplates on mica substrates is due to the electrostatic interaction between the Se^{2-} layer and the K^+ layer. DFT calculations show that a seed layer of Bi_2O_3 can change the contact surface with the substrate significantly (details in the Supporting Information). The calculations of the bare surface energies of Bi_2O_3 are listed in **Table 1**. It is clear that Bi_2O_3 with (111) surface is the dominant exposed surfaces due to its lowest surface energy. The surface crystal structure is shown in Figure 1d. The calculated adhesion energy of Bi_2O_3-(111) covered mica-(001) is 6.055 eV per unit cell, which demonstrates that Bi_2O_3-(111) surface can be adhered steadily to the mica substrate. The Bi_2O_3-(111) surface stacked by Bi_2O_2Se-(100) surface has lower adhesion energy (–1.314 eV per unit cell), compared to that by Bi_2O_2Se-(001) surface (–1.194 eV per unit cell), due to the smaller crystallographic disregistry between Bi_2O_3-(111) and Bi_2O_2Se-(100) (δ = 3.58%) than that between Bi_2O_3-(111) and Bi_2O_2Se-(001) (δ = 4.14%). Therefore, the Bi_2O_2Se-(100) surface is preferentially deposited on Bi_2O_3-(111) surface. As the surface energy of Bi_2O_2Se-(100) (0.891 J m^{-2}) is higher than that of Bi_2O_2Se-(001) (0.823 J m^{-2}), growth of Bi_2O_2Se nanoplates

Table 1. DFT calculated surface energies σ (J m^{-2}) for seven common bare surfaces of Bi_2O_3.

Surface	Surface energy σ (J m^{-2})
(100)	1.132
(010)	1.777
(001)	0.941
(110)	1.057
(101)	1.191
(011)	1.330
(111)	0.892

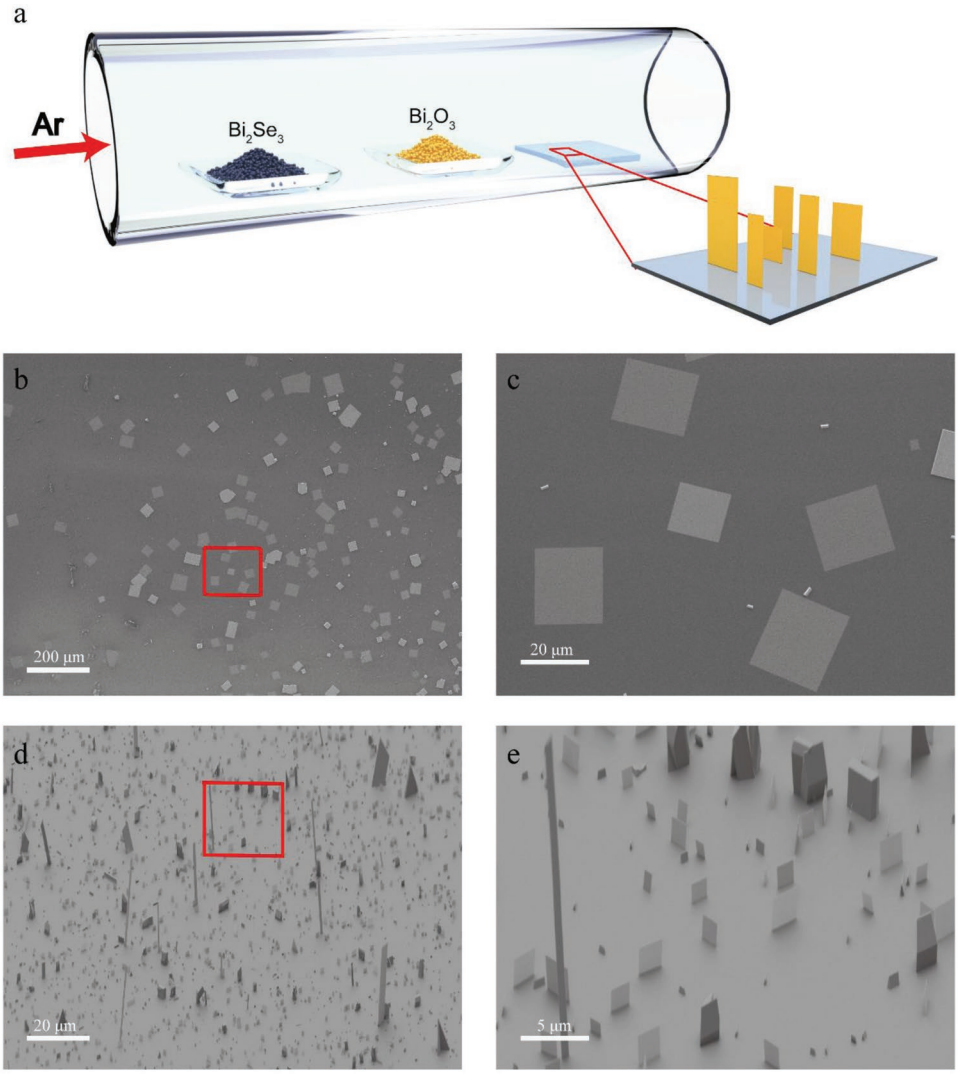

Figure 2. a) Schematic illustration of a CVD setup to synthesize vertical Bi_2O_2Se nanoplates on mica with the coevaporation sources of Bi_2O_3 and Bi_2Se_3. b) SEM images of planar Bi_2O_2Se without a seed layer. c) Magnified view of planar Bi_2O_2Se without a seed layer. d) SEM images of vertical grown Bi_2O_2Se nanoplates with a seed layer. e) Magnified view of vertical grown Bi_2O_2Se nanoplates with a seed layer.

extending along with (100) directions perpendicular to Bi_2O_3 layers is preferred (details in the Supporting Information).

Both syntheses of the planar and vertical nanoplates are accomplished in a tube furnace by coevaporation of Bi_2O_3 powder (99.999%, Alfa Aesar) and Bi_2Se_3 powder (99.999%, Alfa Aesar) at 620 °C for 50 min (details in the Supporting Information). It is found that while there exists a wide window for successful growth of Bi_2O_2Se nanoplates, the growth mode changes dramatically with different amounts of Bi_2O_3. With an atomic ratio of ≈2:1 of Bi_2O_3 and Bi_2Se_3, plane-growth of Bi_2O_2Se nanoplates on mica substrate is realized (**Figure 2**b,c), which is consistent with previous studies.[30] Meanwhile, slightly excessive Bi_2O_3 (an atomic ratio of ≈2.5:1 of Bi_2O_3 and Bi_2Se_3) induces the vertical growth of Bi_2O_2Se nanoplates (Figure 2d,e), which is consistent with our DFT calculations. The existence of the seed of Bi_2O_3 is confirmed by the use of Energy-dispersive X-ray spectroscopy (EDS) analysis of two different parts of Bi_2O_2Se nanoplates and the high-resolution transmitting electron microscopy (HRTEM) of the root of a vertical growing Bi_2O_2Se nanoplate, as shown in Figures S2 and S3 (Supporting Information). It is clear that the oxygen content close to the root of nanoplates is significantly higher compared to that of the central part of nanoplates. Furthermore, different crystal lattices on both sides of the grain boundary indicate two different compounds in the HRTEM image of the root of a Bi_2O_2Se nanoplate. The crystal on the left indicates lattice spacing of 0.25 nm, consistent with the theoretical value of lattice constant of (100) Bi_2O_3. The crystal lattice on the right showed a high-quality Bi_2O_2Se with the lattice constant of (110). Besides, the angle (29°) between the layer of Bi_2O_3 and the grain boundary also agrees with the DFT calculation. For the rest part of this work, all the Bi_2O_2Se nanoplates refer to those vertical grown ones.

With minimized binding with mica substrates, the vertical grown Bi_2O_2Se nanoplates can be conveniently transferred (**Figure 3**a) by a tungsten probe for materials characterizations

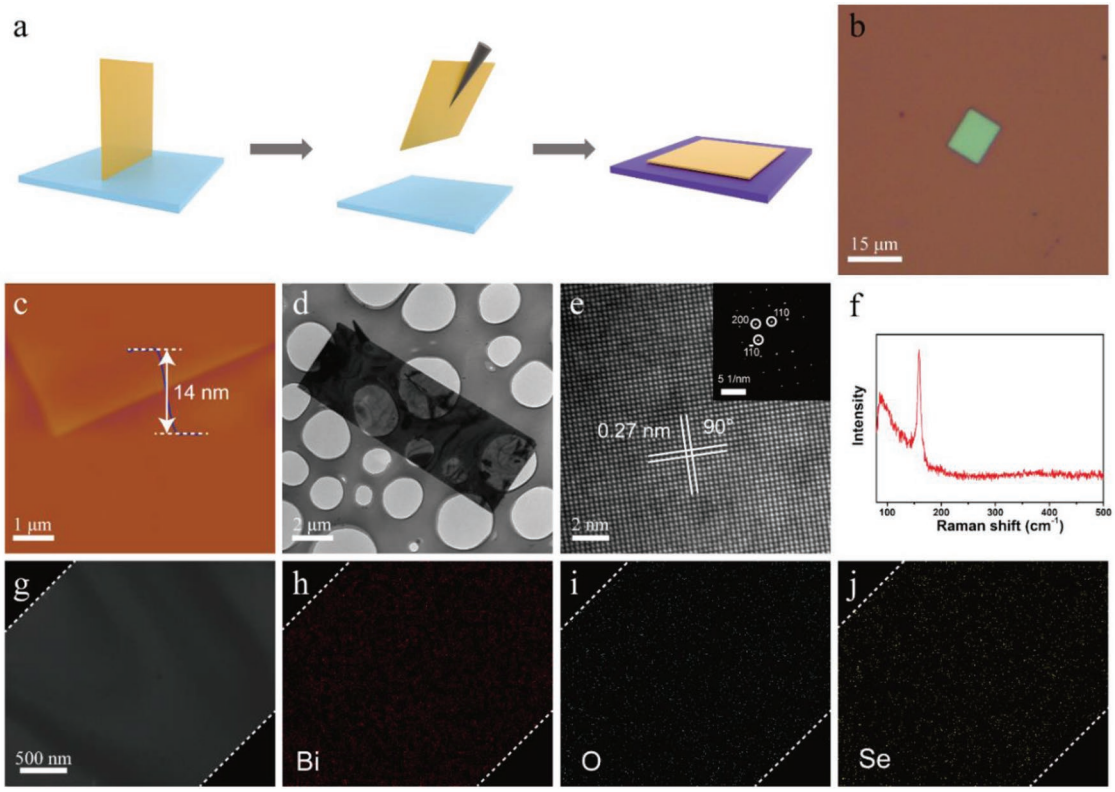

Figure 3. a) Schematic of transfer of vertical grown 2D Bi_2O_2Se nanoplates. b) Photographs of a Bi_2O_2Se nanoplate on the 285 nm SiO_2/Si wafer after transfer. c) AFM topography of a 14 nm thick Bi_2O_2Se nanoplate. d) Low-magnification TEM image of a vertical growing Bi_2O_2Se nanoplate after transferred onto a holey carbon TEM grid. e) HRTEM image of Bi_2O_2Se nanoplate projected along the c-axis and inset shows a SAED pattern. f) Raman shift of 2D Bi_2O_2Se nanoplate. g–j) TEM image of 2D Bi_2O_2Se nanoplates g) and corresponding elemental maps for Bi h), O i), and Se j).

and device fabrications. Figure 3b shows a typical Bi_2O_2Se nanoplate transferred to a SiO_2/Si substrate without any observable damage. Atomic force microscopy (AFM) image shows that the thickness of this Bi_2O_2Se nanoplate is ≈14 nm.

Transmitting electron microscope (TEM) (Figure 3d) was used to further examine the crystal structure and lattice parameter. HRTEM image (Figure 3e) clearly indicates that lattice spacing of 0.27 nm, consistent with the theoretical value of lattice constant of (110) Bi_2O_2Se.[21–31] The selected area diffraction (SAED) pattern (inset) confirms the high crystal quality with tetragonal structure of the Bi_2O_2Se nanoplate. Raman spectrum by a 632.8 nm laser demonstrates the characteristic A_{1g} peak position (≈159 $cm^{-1)}$ of vertical grown Bi_2O_2Se nanoplate (Figure 3f), consistent with the prior works.[29,30] TEM image of a typical Bi_2O_2Se nanoplate and its corresponding EDS element mappings were presented in Figure 3g–j, which confirm the uniform stoichiometry of Bi_2O_2Se nanoplate.

Bi_2O_2Se nanoplates are considered as a promising thermoelectric material according to previous theoretical calculations.[33,34] For example, first-principles study has predicted ultralow lattice thermal conductivity in 2D structures of Bi_2O_2Se,[34] due to low phonon group velocity and large Gruñeisen parameters. However, thermal measurement of individual Bi_2O_2Se nanoplate has not been explored as it has been difficult to exclude the effect from the substrate. Vertical grown Bi_2O_2Se nanoplates, which can be conveniently transferred to suspended membranes,[35] are ideal candidates for thermal conductivity measurement with the developed Wheatstone bridge circuit,[36] as shown in **Figure 4**a.

Figure 4b shows the measured thermal conductivity of a typical Bi_2O_2Se nanoplate (26.8 nm thick), in comparison with those of traditional thermoelectric materials Bi_2Se_3,[37] bulk Bi_2O_2Se,[38] and monolayer Bi_2O_2Se from theoretical calculations.[34] As Bi_2O_2Se is formed out of reaction between Bi_2Se_3 and Bi_2O_3. Bi_2O_2Se possess weak bonding between Se^{2-} layer and $[Bi_2O_2]^{2+}$ layer, which leads to quite different phonon dispersion from Bi_2Se_3. Theoretical calculations for phonon dispersion of bulk Bi_2O_2Se indicate that it has lower frequency of optical branch than typical thermoelectric material.[34] Combined soften optical mode and low acoustic phonon velocity in Bi_2O_2Se, we can see that thermal conductivity of Bi_2O_2Se (e.g., 0.92 W m^{-1} K^{-1} at 50 K) is lower than Bi_2Se_3 nanoribbon (4.03 W m^{-1} K^{-1} at 50 K) at low temperature. Furthermore, large atom mass difference between Bi and O can lead to larger phonon bandgap. This can further suppress phonon Umklapp scattering.[39,40] Therefore, there is no obvious Umklapp peak observed in our Bi_2O_2Se nanoplate, drastically different from that of Bi_2Se_3 nanoplate.

At room temperature and above, thermal conductivity of this Bi_2O_2Se nanoplate is comparable to that of bulk Bi_2O_2Se. The thermal conductivity of our Bi_2O_2Se nanoplate is about 1 W m^{-1} K^{-1} at 300 K. As theoretical calculations indicate that Bi_2O_2Se has short phonon mean free path,[34] it is expected that classic size effect plays little role on thermal conductivity of

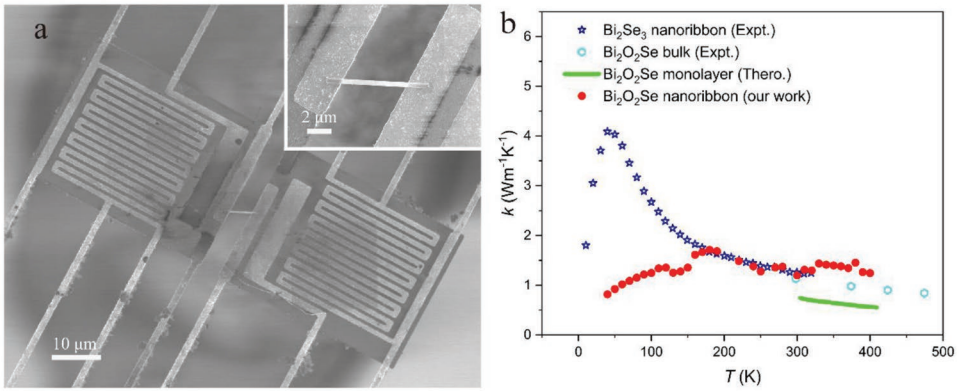

Figure 4. a) SEM micrograph of the 2D Bi_2O_2Se nanoplate on suspended membrane for thermalconductivity measurement. b) Thermal conductivity of a Bi_2O_2Se nanoplate, in comparison with Bi_2Se_3 nanoribbon (ref. [37]), Bi_2O_2Se bulk (ref. [38]), and Bi_2O_2Se monolayer (theoretical calculations, ref. [34]).

Bi_2O_2Se. As thermal conductivity of monolayer Bi_2O_2Se from theoretical calculations is significantly lower than those of the measured nanoplates and bulk counterparts, it can be expected that the modified phonon dispersion in monolayer Bi_2O_2Se with low phonon velocity is more favorable for thermoelectric applications.

3. Conclusion

In summary, through both theoretical calculations and experiments, we demonstrate a seed-induced vertical growth of 2D layered materials. As an example, vertical Bi_2O_2Se nanoplates can be grown on mica substrate, with Bi_2O_3 serving as seeds at nucleation stage of growth. These vertical grown 2D nanoplates, with minimized bonding with substrate, can be conveniently transferred for probing fundamental properties and constructing advanced devices. As a result, we reported the first thermal conductivity measurement of those Bi_2O_2Se nanoplates, which demonstrates the great potential for thermoelectric applications.

Supporting Information

Supporting Information is available from the Wiley Online Library or from the author.

Acknowledgements

Z.W., G.L., Y.W., and X.Y. contributed equally to this work. The authors acknowledge the microfabrication center of National Laboratory of Solid State Microstructures (NLSSM) for technique support. This work is supported by the State Key Program for Basic Research of China (No. 2015CB659300), National Natural Science Foundation of China (Nos. 21805132, 11574143, 11874211, 11621091, and 61735008), Natural Science Foundation of Jiangsu Province (No. BK20180341), and the Fundamental Research Funds for the Central Universities (Nos. 021314380135 and 021314380128).

Conflict of Interest

The authors declare no conflict of interest.

Keywords

Bi_2O_2Se, seed growth, thermal properties, 2D layered materials, vertical growth

Received: August 13, 2019
Revised: September 9, 2019
Published online:

[1] Y. Chen, Z. Fan, Z. Zhang, W. Niu, C. Li, N. Yang, B. Chen, H. Zhang, *Chem. Rev.* **2018**, *118*, 6409.
[2] M. Nasilowski, B. Mahler, E. Lhuillier, S. Ithurria, B. Dubertret, *Chem. Rev.* **2016**, *116*, 10934.
[3] C. Tan, X. Cao, J. X. Wu, Q. He, J. Yang, X. Zhang, J. Chen, W. Zhao, S. Han, G. H. Nam, M. Sindoro, H. Zhang, *Chem. Rev.* **2017**, *117*, 6225.
[4] X. Yang, X. Dou, A. Rouhanipour, L. Zhi, H. J. Rader, K. Mullen, *J. Am. Chem. Soc.* **2008**, *130*, 4216.
[5] Y. Wang, N. Xu, D. Li, J. Zhu, *Adv. Funct. Mater.* **2017**, *27*, 1604134.
[6] K. S. Novoselov, A. Mishchenko, A. Carvalho, A. H. Castro Neto, *Science* **2016**, *353*, aac9439.
[7] M. Xu, T. Liang, M. Shi, H. Chen, *Chem. Rev.* **2013**, *113*, 3766.
[8] Y. Zhang, L. Zhang, C. Zhou, *Acc. Chem. Res.* **2013**, *46*, 2329.
[9] G. Fiori, F. Bonaccorso, G. Iannaccone, T. Palacios, D. Neumaier, A. Seabaugh, S. K. Banerjee, L. Colombo, *Nat. Nanotechnol.* **2014**, *9*, 768.
[10] J. Wang, H. Zheng, G. Xu, L. Sun, D. Hu, Z. Lu, L. Liu, J. Zheng, C. Tao, L. Jiao, *J. Am. Chem. Soc.* **2016**, *138*, 16216.
[11] B. Zhao, W. Dang, Y. Liu, B. Li, J. Li, J. Luo, Z. Zhang, R. Wu, H. Ma, G. Sun, Y. Huang, X. Duan, X. Duan, *J. Am. Chem. Soc.* **2018**, *140*, 14217.
[12] M. T. Pettes, I. Jo, Z. Yao, L. Shi, *Nano Lett.* **2011**, *11*, 1195.
[13] Y. C. Lin, C. C. Lu, C. H. Yeh, C. Jin, K. Suenaga, P. W. Chiu, *Nano Lett.* **2012**, *12*, 414.
[14] I. Jo, M. T. Pettes, J. Kim, K. Watanabe, T. Taniguchi, Z. Yao, L. Shi, *Nano Lett.* **2013**, *13*, 550.
[15] J. Kang, D. Shin, S. Bae, B. H. Hong, *Nanoscale* **2012**, *4*, 5527.
[16] X. S. Li, Y. W. Zhu, W. W. Cai, M. Borysiak, B. Y. Han, D. Chen, R. D. Piner, L. Colombo, R. S. Ruoff, *Nano Lett.* **2009**, *9*, 4359.
[17] X. L. Liang, B. A. Sperling, I. Calizo, G. J. Cheng, C. A. Hacker, Q. Zhang, Y. Obeng, K. Yan, H. L. Peng, Q. L. Li, X. X. Zhu, H. Yuan, A. R. H. Walker, Z. F. Liu, L. M. Peng, C. A. Richter, *ACS Nano* **2011**, *5*, 9144.
[18] H. Ci, H. Chang, R. Wang, T. Wei, Y. Wang, Z. Chen, Y. Sun, Z. Dou, Z. Liu, J. Li, P. Gao, Z. Liu, *Adv. Mater.* **2019**, *31*, 1901624.

[19] Y. Teng, H. Zhao, Z. Zhang, Z. Li, Q. Xia, Y. Zhang, L. Zhao, X. Du, Z. Du, P. Lv, K. Świerczek, *ACS Nano* **2016**, *10*, 8526.
[20] Y. Jiang, X. Zhang, Y. Wang, N. Wang, D. West, S. Zhang, Z. Zhang, *Nano Lett.* **2015**, *15*, 3147.
[21] J. Wu, Y. Liu, Z. Tan, C. Tan, J. Yin, T. Li, T. Tu, H. Peng, *Adv. Mater.* **2017**, *29*, 1704060.
[22] J. Yin, Z. Tan, H. Hong, J. Wu, H. Yuan, Y. Liu, C. Chen, C. Tan, F. Yao, T. Li, Y. Chen, Z. Liu, K. Liu, H. Peng, *Nat. Commun.* **2018**, *9*, 3311.
[23] J. Li, Z. Wang, Y. Wen, J. Chu, L. Yin, R. Cheng, L. Lei, P. He, C. Jiang, L. Feng, J. He, *Adv. Funct. Mater.* **2018**, *28*, 1706437.
[24] Q. Fu, C. Zhu, X. Zhao, X. Wang, A. Chaturvedi, C. Zhu, X. Wang, Q. Zeng, J. Zhou, F. Liu, B. K. Tay, H. Zhang, S. J. Pennycook, Z. Liu, *Adv. Mater.* **2019**, *31*, 1804945.
[25] U. Khan, Y. Luo, L. Tang, C. Teng, J. Liu, B. Liu, H. M. Cheng, *Adv. Funct. Mater.* **2019**, *29*, 1807979.
[26] Z. Zhang, T. Li, Y. Wu, Y. Jia, C. Tan, X. Xu, G. Wang, J. Lv, W. Zhang, Y. He, J. Pei, C. Ma, G. Li, H. Xu, L. Shi, H. Peng, H. Li, *Adv. Mater.* **2019**, *31*, 1805769.
[27] J. Wu, C. Qiu, H. Fu, S. Chen, C. Zhang, Z. Dou, C. Tan, T. Tu, T. Li, Y. Zhang, Z. Zhang, L. Peng, P. Gao, B. Yan, H. Peng, *Nano Lett.* **2019**, *19*, 197.
[28] H. X. Fu, J. X. Wu, H. L. Peng, B. H. Yan, *Phys. Rev. B: Condens. Matter Mater. Phys.* **2018**, *97*, 5.
[29] J. Wu, H. Yuan, M. Meng, C. Chen, Y. Sun, Z. Chen, W. Dang, C. Tan, Y. Liu, J. Yin, Y. Zhou, S. Huang, H. Q. Xu, Y. Cui, H. Y. Hwang, Z. Liu, Y. Chen, B. Yan, H. Peng, *Nat. Nanotechnol.* **2017**, *12*, 530.
[30] J. Wu, C. Tan, Z. Tan, Y. Liu, J. Yin, W. Dang, M. Wang, H. Peng, *Nano Lett.* **2017**, *17*, 3021.
[31] C. Chen, M. Wang, J. Wu, H. Fu, H. Yang, Z. Tian, T. Tu, H. Peng, Y. Sun, X. Xu, J. Jiang, N. B. M. Schroter, Y. Li, D. Pei, S. Liu, S. A. Ekahana, H. Yuan, J. Xue, G. Li, J. Jia, Z. Liu, B. Yan, H. Peng, Y. Chen, *Sci. Adv.* **2018**, *4*, eaat8355.
[32] X. Yang, X. Li, Y. Deng, Y. Wang, G. Liu, C. Wei, H. Li, Z. Wu, Q. Zheng, Z. Chen, Q. Jiang, H. Lu, J. Zhu, *Adv. Funct. Mater.* **2019**, *29*, 1902427.
[33] H. Y. Song, X. J. Ge, M. Y. Shang, J. T. Lü, preprint arXiv:1901.01490 **2019**.
[34] X. L. Zhu, P. F. Liu, G. Xie, B. T. Wang, *Phys. Chem. Chem. Phys.* **2019**, *21*, 10931.
[35] D. Li, Y. Wu, P. Kim, L. Shi, P. Yang, A. Majumdar, *Appl. Phys. Lett.* **2003**, *83*, 2934.
[36] J. Zheng, M. C. Wingert, E. Dechaumphai, R. Chen, *Rev. Sci. Instrum.* **2013**, *84*, 114901.
[37] H. Tang, X. Wang, Y. Xiong, Y. Zhao, Y. Zhang, Y. Zhang, J. Yang, D. Xu, *Nanoscale* **2015**, *7*, 6683.
[38] B. Zhan, Y. C. Liu, X. Tan, J. L. Lan, Y. H. Lin, C. W. Nan, *J. Am. Ceram. Soc.* **2015**, *98*, 2465.
[39] L. Lindsay, D. A. Broido, T. L. Reinecke, *Phys. Rev. Lett.* **2013**, *111*, 025901.
[40] S. K. Saha, G. Dutta, *Phys. Rev. B* **2016**, *94*, 125209.